

# Free Energy and Structure of Dislocation Cores in Two-Dimensional Crystals<sup>†</sup>

P. B. Bladon<sup>‡</sup> and D. Frenkel\*

FOM Institute for Atomic and Molecular Physics, Kruislaan 407, 1098 SJ Amsterdam, The Netherlands

Received: October 2, 2003

The nature of the melting transition in two dimensions is critically dependent on the core energy of dislocations. In this paper, we report calculations of the core free energy and the core size of dislocations in two-dimensional solids of systems interacting via square well, hard disk, and  $r^{-12}$  potentials. In all cases, we find that the dislocation core free energy is such that, at the densities studied, the density of free dislocation density is extremely low. We find that the core energies and core sizes are considerably smaller for the  $r^{-12}$  system than for the other systems studied. This illustrates the fact that, for hard-core systems, elastic continuum theory breaks down, even for relatively small strains.

## 1. Introduction

The debate about the nature of the melting transition in (quasi) two-dimensional (2D) systems dates back to the seminal work of Landau and Peierls, who showed that there is no long-range positional order in 2D crystals (see, e.g., ref 1). In the early 1970s, Kosterlitz and Thouless suggested that melting in two dimensions might proceed via a continuous dislocation-unbinding transition.<sup>2</sup> Subsequently, Halperin and Nelson<sup>3</sup> argued that the phase resulting after dislocation unbinding is not an isotropic liquid, because it still has quasi-long-range bond-orientational order. A second (disclination unbinding) transition is required to obtain an isotropic liquid from the bond-ordered phase (termed “hexatic” in ref 3). These predictions have stimulated a great amount of experimental, theoretical, and numerical work on melting in 2D systems, most recently reviewed by Glaser and Clark<sup>4</sup> and Strandburg.<sup>5</sup> Experimental work on colloids and smectic thermotropic liquid crystals has found evidence that supports the dislocation unbinding theory. However, the verification of the original theoretical predictions by computer simulation has been much more difficult than originally envisaged, because of the difficulty of investigating systems very close to melting. The investigation of melting in two dimensions still remains a very active research area, both experimentally (in colloids,<sup>12–17</sup> vortex flux lattices<sup>18,19</sup> and free-standing liquid-crystalline films<sup>20</sup>) and numerically.<sup>6–11,21–27</sup>

One reason the debate about the nature of the 2D melting transition is still continuing is that it is extremely difficult to distinguish between a weak, first-order melting transition and a continuous transition. The problem is that it is very hard to determine if the point where a solid becomes unstable toward dislocation unbinding is pre-empted by simple first-order melting. And, even if it is, it is difficult to determine if that melting transition directly transforms the system to an isotropic liquid. One reason the picture is so unclear is that existing theories for dislocation unbinding assume that the number of defects in the solid at melting is low. However, in practice, it seems that a solid that is close to melting contains many defects. This is presumably related to the fact that the “core (free)

energy” of a dislocation is often rather low. In fact, there is evidence<sup>28,29</sup> that no continuous dislocation-unbinding transition is possible if the core (free) energy of a dislocation is less than  $\sim 3k_B T$ .

In this paper, we primarily focus on systems where no such confusion exists: we consider a model solid that can become unstable to dislocation unbinding far away from any first-order melting curve. Such dislocation-unbinding transitions should occur in 2D solids of particles with a short-range attraction or a “shoulder-like” repulsion. These systems can undergo an isostructural solid–solid transition, and, near the solid–solid critical point, there should be a “pocket” in the phase diagram where the hexatic phase is stable<sup>30</sup> termination of a line of first-order isostructural solid phase coexistence. The size and location of the region is sensitively dependent on the range of attraction of the pair potential. Because of the low dislocation density in this unstable region, the resulting phase satisfies all the criteria of a stable hexatic.<sup>30,31</sup> Moreover, such systems are not purely of theoretical interest, because there is experimental evidence that short-range attraction or repulsions can favor the formation of hexatic phases<sup>13–15,26</sup> The simulations of ref 30 showed that the defect concentration in the solid, at the putative solid-hexatic transition, was extremely low. This suggests that the core free energy of dislocations is large, compared to  $k_B T$ . In the present paper, we show that this is indeed the case. In particular, we compute the core free energy of a pair of dislocations for our model system—the attractive square-well system—and two other model systems (namely, the hard disk solid and a system interacting via a repulsive  $r^{-12}$  potential). To our knowledge, this is the first time that the core free energy has been calculated directly; previous calculations were based either on a quasi-harmonic approximation that neglects part of the entropic contribution to the dislocation free energy<sup>32</sup> or the entropic contribution was completely neglected.<sup>33</sup> Our calculations give a more quantitative indication of the dislocation density and highlight the qualitative difference of systems with and without a hard core. The very high defect core free energies calculated for the square-well system indicate that it may be impossible to directly observe free dislocations in a hexatic phase (of the type studied) by computer simulation, at least on currently available computers. However, this does not rule out the experimental observation of hexatic phases induced by the same

<sup>†</sup> Part of the special issue “Hans C. Andersen Festschrift”.

\* Author to whom correspondence should be addressed. E-mail address: frenkel@amolf.nl.

<sup>‡</sup> Present address: Marconi Communications Ltd., Coventry, U.K.

mechanism, because accessible experimental length scales can be much greater than those of a simulation.

The remainder of the paper is divided as follows. First, we give a brief resumé of the dislocation unbinding theory of melting and its main predictions. We then show how the presence of a critical point in the solid phase can lead to dislocation unbinding in the solid far from melting. We present computer simulations to show that the area of unstable solid in the phase diagram is sensitively dependent on the form of the intermolecular potential. Finally, we explain, in some detail, the procedure used to measure the core free energy of a dislocation.

## 2. Dislocation Mediated Melting in Two Dimensions

The dislocation-unbinding theory of melting that was developed by Kosterlitz, Thouless, Halperin, Nelson, and Young (the KTHNY theory), is based on the linear elasticity theory of an isotropic medium. This encompasses all 2D, substrate-free systems that crystallize in a triangular lattice. Because of the 6-fold symmetry, such lattices possess only two distinct elastic constants.<sup>34</sup> In two dimensions, there are only two types of defects that can occur: dislocations and disclinations.<sup>35</sup> Disclinations have a very severe effect on the lattice structure and, consequently, a high free energy. Only dislocations are relevant to melting in two dimensions. Kosterlitz and Thouless<sup>2</sup> presented a simple argument to explain why a solid should melt via a dislocation-unbinding transition, based on the free energy of an isolated dislocation. The energy of an isolated dislocation calculated via continuum theory is

$$U = \frac{K}{16\pi} \ln\left(\frac{A}{a_0^2}\right) \quad (1)$$

where  $A$  is the size of the system,  $a$  is some characteristic size of the dislocation,  $a_0$  is the lattice constant, and  $K$  is the combination of Lamé coefficients, given by

$$K = \frac{4a_0^2\mu(\mu + \lambda)}{2\mu + \lambda} \quad (2)$$

There are approximately  $A/(a_0^2)$  locations for the dislocation; therefore, entropy must have the form  $S = k_B \ln[A/(a_0^2)]$ . The total free energy of a single dislocation is then given, within a constant, by

$$\mathcal{F} \approx \left(\frac{K}{16\pi} - k_B T\right) \ln\left(\frac{A}{a_0^2}\right) \quad (3)$$

When  $K/(16\pi) \leq k_B T$ , dislocations proliferate and the translational order of the solid is destroyed. Kosterlitz and Thouless calculated the effect of scalar-type dislocations on the solid phase. The full vector nature of the dislocation interaction was considered by Halperin and Nelson,<sup>3</sup> and additional predictions were made by Young.<sup>36</sup>

These treatments begin by considering the free energy of an elastic solid described by a strain tensor  $u_{ij}$ :

$$\frac{\mathcal{F}}{k_B T} = \frac{1}{2} \int \frac{d^2 r}{a_0^2} (2\bar{\mu} u_{ij}^2 + \bar{\lambda} u_{kk}^2) \quad (4)$$

$\bar{\lambda}$  and  $\bar{\mu}$  are the Lamé elastic constants of the lattice, divided by  $k_B T$  and multiplied by  $a_0^2$ , i.e.,  $\bar{\mu} = \mu a_0^2 / (k_B T)$  and  $\bar{\lambda} = \lambda a_0^2 / (k_B T)$ . Henceforth, we shall drop the overline and assume that all elastic constants are expressed in these reduced units.

In the presence of dislocations, the strain field  $u_{ij}$  can be expressed as the sum of a smoothly varying part ( $\phi_{ij}$ ) that is due to the phonon modes and a singular part ( $u_{ij}^{\text{sing}}$ ) that is due to point dislocations:

$$u_{ij} = \phi_{ij} + u_{ij}^{\text{sing}} \quad (5)$$

This causes the free energy to separate into three parts:

$$\mathcal{F} = \mathcal{F}_0 + \mathcal{F}_D + \mathcal{F}_c \quad (6)$$

where  $\mathcal{F}_0$  describes the smoothly varying strains,

$$\frac{\mathcal{F}_0}{k_B T} = \frac{1}{2} \int \frac{d^2 r}{a_0^2} (2\mu \phi_{ij}^2 + \lambda \phi_{kk}^2) \quad (7)$$

and  $\mathcal{F}_D$  is the contribution from the dislocations,

$$\frac{\mathcal{F}_D}{k_B T} = -\frac{K}{8\pi} \sum_{r_i \neq r_j} \left[ \mathbf{b}_i \cdot \mathbf{b}_j \ln\left(\frac{r_{ij}}{a_0}\right) - \frac{(\mathbf{b}_i \cdot \mathbf{r}_{ij})(\mathbf{b}_j \cdot \mathbf{r}_{ij})}{r_{ij}^2} \right] \quad (8)$$

where  $\mathbf{b}_i$  denotes the Burger's vector (see below) of dislocation  $i$ . The dislocation contribution to the free energy (eq 8) results from an integration of the strain field outside a contour of radius  $a$  from the point dislocation. The strain field near a dislocation varies rapidly. In fact, at the dislocation itself, there is a discontinuity in the displacement field and near it, the lattice is ill-defined, as are displacements from the lattice.<sup>35</sup> Yet, the contribution to the free energy that is due to the distortion of the lattice inside the radius  $a$  is necessarily finite; it is assumed to be a constant (at a given thermodynamic state point). As a result, the dislocation cores yield a separate contribution to the free energy of the system. This contribution is called the core free energy,  $\mathcal{F}_c$ :

$$\mathcal{F}_c = \frac{E_c}{k_B T} \sum_{\mathbf{b}_i} \mathbf{b}_i^2 \quad (9)$$

Dislocations are uniquely described by a Burger's vector  $\mathbf{b}$ , which is defined as the amount by which a Burger's circuit (a circuit that would close in a perfect triangular lattice) around the dislocation fails to close. The Burger's vector is measured in units of the lattice spacing; the magnitude indicates the strength of the dislocation. A suitable microscopic definition of a Burger's vector is discussed in Section 4.3.

As eq 8 shows, the free energy of a dislocation pair diverges logarithmically with the system size. In a system with many dislocations, the dislocations screen each other and the free energy is only finite if the constraint  $\sum_i \mathbf{b}_i = 0$  is satisfied, i.e., dislocations are produced in pairs. In the theories of Halperin and Nelson and Young, the effect of dislocation screening is to renormalize the elastic constants  $\mu$ ,  $\lambda$ , and  $K$ . The contribution of the dislocations to the elastic constants is calculated as a power series in  $y = e^{-E_c/(k_B T)}$ .

A summary of the predictions of the theory are as follows:

(1) Dislocations unbind, forming a phase that Halperin and Nelson called "hexatic", at a temperature  $T = T_m$  when the renormalized elastic constant  $K_R(T)$  approaches  $16\pi$  from above as  $T$  approaches the melting temperature  $T_m$  from below. This is exactly the same result as the simple entropy/energy argument given by Kosterlitz and Thouless, but with  $K$  renormalized.

(2) The hexatic phase-density-density correlation function decays exponentially as the correlation length  $\xi$  increases,

diverging as  $T$  approaches  $T_m$  from above:

$$\langle \rho(r)\rho(0) \rangle \approx \exp\left(-\frac{r}{\xi(T)}\right) \quad (10)$$

(3) The correlation of a bond orientational order parameter ( $\Psi_6 = e^{i6\theta}$ , where  $\theta$  is the angle that suitably chosen nearest neighbors make with a reference axis) decay algebraically above  $T_m$ , with  $\eta_6$  rapidly going to zero as  $T$  approaches  $T_m$  from above:

$$\langle \Psi_6(r)\Psi_6(0) \rangle \approx r^{-\eta_6(T)} \quad (11)$$

(4) The hexatic phase melts via an unbinding of disclination pairs to become an isotropic liquid (a free dislocation can be considered as a bound pair of disclinations). We shall not concern ourselves further with the disclination-unbinding transition in this article.

The hexatic phase, then, has an exponential decay of translational correlations, with a slow (algebraic) decay of bond-angle correlations. The free energy contains an essential singularity at the transition, so there are no discontinuities in any thermodynamic function; in effect, the transition is the point where dislocations start to become unbound. The concentration of free dislocations at this point is zero.

All microscopic information about the solid is contained in the elastic constants of the material and the core energy of the dislocation. The elastic constants measure the *free-energy* cost of imposing a given set of strains on the system. Even a hard particle system will exhibit an elastic response, because of the entropy reduction of a distortion.

It is important to realize that the two-stage melting mechanism does not prohibit the solid from melting before the solid becomes unstable to dislocation unbinding. Only if the solid is thermodynamically stable at the dislocation proliferation instability will the subtle dislocation unbinding result. Many other melting scenarios have been proposed (for a review, see ref 4). Among these, the grain-boundary-melting scenarios have received special attention. Fisher<sup>33</sup> found that the spontaneous proliferation of grain boundaries would be unfavorable, compared to dislocation formation; however, a more detailed calculation by Chui<sup>28</sup> suggested that if the core energy ( $E_c$ ) were low enough ( $< 2.84k_B T$ ), then melting would proceed via a (first-order) proliferation of grain boundaries (although, strictly speaking, it is not meaningful to speak about the “mechanism” of a first-order phase transition). Grain boundaries completely destroy the bond-orientational order of the system, so that no hexatic phase occurs. For larger values of the core energy ( $E_c > 2.84k_B T$ ), the transition becomes much more weakly first-order. Interestingly, these predictions were supported by a simulation of the equivalent lattice Hamiltonian to eq 6 by Saito,<sup>29</sup> who found that the melting transition is first-order for small core energies and continuous for large core energies, with a crossover between  $E_c = 2.28k_B T$  and  $E_c = 3.28k_B T$ . Saito also observed that melting is caused by dislocation unbinding at high core energies, whereas the formation of grain boundaries is observed at lower core energies. Therefore, it seems that the core energy does indeed have an important role in determining the melting behavior.

There have also been many computer experiments that have examined melting in two dimensions. Many different systems have been investigated, including hard disks and power-law potentials ( $r^{-12}$ ,  $r^{-6}$ ,  $r^{-5}$ ,  $r^{-3}$ ,  $r^{-1}$ , logarithmic, Yukawa, Lennard-Jones and Weeks–Chandler–Andersen potentials). A computer experiment initially might seem to be the ideal tool

to search for two-stage melting and the hexatic phase. There is absolute control over the experimental conditions, and parameter space can be rigorously searched. The simulations are in two dimensions—and, therefore, fast—and systems of relatively large spatial extent can be studied. However, despite the great amount of work and computer time that have been invested in simulating model systems, it has proven to be unexpectedly difficult to obtain hard evidence for (or against) the existence of a hexatic phase by computer simulation. The main reason for this difficulty is that, near the transition region, the presence of topological defects dramatically slows equilibration, which makes it difficult to precisely identify any transition, be it first-order or otherwise. There have recently been several large simulations of 2D solids, only one of which found evidence for a thermodynamically stable hexatic phase. Chen et al.<sup>8</sup> studied a large Lennard-Jones system in the *NPT* ensemble and found evidence only for a metastable hexatic phase. Bagchi et al.<sup>11</sup> identified a stable hexatic phase in a large (64 000 particle) simulation of a repulsive  $r^{-12}$  potential, using a bicononical technique<sup>37</sup> to accelerate the equilibration of defects. The range of stability of this hexatic phase was quite narrow ( $\sim 1.2\%$  of the accessible density range). Weber and Marx<sup>6</sup> and Fernández<sup>10</sup> studied large hard disk systems, with Weber and Marx finding evidence for a first-order transition with a very narrow coexistence region, whereas Fernández et al. found a single continuous transition. However, even for a system as simple as hard disks, the situation is, even now, far from clear.<sup>22–25,27</sup>

There are alternatives to direct observation of the correlation functions that are characteristic of a hexatic phase. One may look at the elastic constants of the system and determine if the solid is unstable, with respect to the KTHNY criterion (i.e.,  $K < 16\pi$ ). If the solid is unstable to dislocation unbinding, then one may infer that an infinitely sized system will be hexatic. This presupposes two things: (i) the system must be thermodynamically stable, and (ii) the assumptions underlying the KTHNY theory should be satisfied (i.e., that the system should be in a regime where the defect core energy is sufficiently high for the expansion in defect fugacity to be valid). Investigations of the location of the hexatic phase, on the basis of elastic constant measurements, conflict with the first argument. It seems that the locus of the elastic constant  $K = 16\pi$  is depressingly close to the point where the solid becomes unstable to first-order melting.<sup>38,39</sup>

In this paper, we are concerned with hexatic phases that occur deep inside the solid phase, where there is less risk of “interference” from the regular melting transition.

### 3. Hexatic Phase in Systems with Short-Range Interactions

The effect of the range of attraction of a simple pairwise additive potential on the phase diagram has received much attention in recent years.<sup>40</sup> Computer simulations, theory, and experiments on colloidal suspensions have shown that the liquid phase is only stable if the range of attraction is greater than  $\sim 30\%$  of the particle diameter. If the range of attraction (measured in some suitable way) is too short, the liquid–gas critical point disappears. Recent work considered the effect of reducing the range of the attractive portion of the potential even further.<sup>41</sup> The surprising conclusion was that if the potential becomes sufficiently short-ranged, a critical point would reappear in the solid phase. The critical point separates two regions of solid, with identical structure but different density (see Figure 1). The low(er)-density solid phase is stabilized by “free

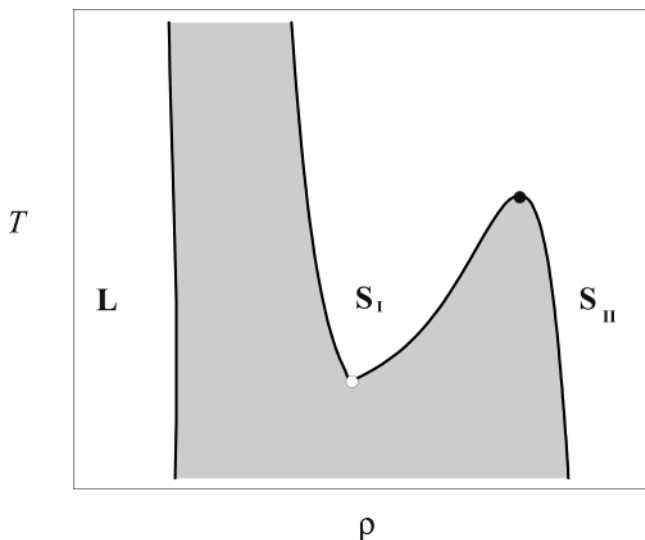


**Figure 1.** Generic phase diagram for the isostructural solid–solid transition in the  $(\rho, T)$  plane. Low-density solid  $S_I$  coexists with a higher density solid  $S_{II}$ , separated by a critical point (marked by a solid circle, ●). The triple point (marked by an open circle, ○), marks the point of the coexistence of  $S_I$ ,  $S_{II}$ , and liquid ( $L$ ). Regions of two-phase coexistence are shaded gray.

volume” entropy, which is the same mechanism that stabilizes a hard sphere solid; the high-density solid is stabilized energetically. Bolhuis and Frenkel studied two systems by computer simulation: the square-well solid in two and three dimensions, and the hard-core plus attractive Yukawa potential in three dimensions. The results for all systems were qualitatively similar, and subsequent theoretical work indicates that the mechanism is quite general; i.e., any attractive potential of sufficiently short range will display a critical point in the solid.<sup>42,43</sup>

What are the implications of a critical point in the solid phase for the dislocation-mediated melting theory? A central prediction of the KTHNY theory is that the solid becomes unstable to dislocation unbinding when the elastic constant is  $K = 16\pi$ . The bulk modulus vanishes at the critical point and can be made arbitrarily small by approaching the critical point. Re-expressing eq 2 in terms of the 2D bulk modulus ( $B = \lambda + \mu$ ) and shear modulus  $\mu$ , near the critical point, we have

$$K = \frac{4\mu B}{\mu + B} \approx 4B \left(1 - \frac{B}{\mu} + \dots\right) \quad (12)$$

As we shall see,  $\mu$  is not strongly affected by a solid–solid critical point. Hence, there will be a finite region around the critical point where  $K$  is dominated by the bulk modulus  $B$  and is less than  $16\pi$ . The solid will, necessarily, become unstable to dislocation unbinding. This mechanism for the formation of a hexatic phase is very similar to one proposed by Toner and Prost in the context of the formation of an induced nematic phase in the vicinity of a Smectic–Smectic critical point.<sup>44</sup> Recently, Chen and Nelson showed that the presence of an Ising-like first-order phase transition in the solid does not interfere with the dislocation-unbinding mechanism.<sup>31</sup>

We have performed computer simulations to map out the region in the phase diagram that is unstable to dislocation unbinding. We studied the 2D attractive square-well model, because the phase diagram of this system is known from the work of Bolhuis and Frenkel.<sup>41</sup> The pair potential in this model

is given by

$$v(r) = \infty \quad (\text{for } 0 \leq r < \sigma) \quad (13a)$$

$$= -\epsilon \quad (\text{for } \sigma \leq r < \sigma + \delta) \quad (13b)$$

$$= 0 \quad (\text{for } r \geq \sigma + \delta) \quad (13c)$$

where  $\sigma$  is the particle diameter,  $\epsilon$  the well depth, and  $\delta$  the well width. Henceforth, we measure all temperatures in units of  $\epsilon/k_B$  and set the particle diameter to a value of 1. The simulations of ref 41 showed that solid–solid coexistence is possible if the width  $\delta$  of the square well is less than  $\sim 7\%$  of the particle diameter. For longer-range attraction, the triple-point temperature becomes greater than the critical-point temperature and the low-density solid disappears. For decreasing  $\delta$ , the solid–solid critical point moves to higher densities, whereas the ratio of the triple-point temperature to the critical temperature decreases. In the limit  $\delta \rightarrow 0$ , the critical density approaches that of regular close packing. By controlling the range of attraction ( $\delta$ ), we can choose the density at which the critical point occurs. This allows us to study systems arbitrarily deep inside the solid phase. A good estimate of where the critical point occurs can be made by calculating the density at which the square wells of adjacent particles that occupy the perfect lattice first overlap. Note that, because we are studying the elastic properties of the solid near the critical point, we can avoid any problems of thermodynamic instability; wherever the bulk modulus  $B$  is positive, the system is stable.

Instead of direct examination of the dislocation unbinding, we chose to identify unstable regions of the solid by calculating the elastic constant  $K$ . The dislocation concentration is strongly dependent on density; therefore, we expect that the dislocations concentration will be very low, because the solid–solid critical point occurs at densities that are significantly greater than the hard-disk melting density. To determine the value of  $K$ , we needed to calculate the elastic constants  $\mu$  and  $\lambda$  as a function of density and temperature. Calculation of elastic constants requires knowledge of the pressure tensor, which is best obtained using a molecular dynamics simulation. We used the technique pioneered by Alder and Wainwright,<sup>45</sup> augmented by a collision list handling technique that is similar to that described by Rapaport<sup>46</sup> to obtain an algorithm that scales as  $N \ln^2 N$ , where  $N$  is the number of particles in the simulation. Constant temperature was maintained using velocity scaling. To check that the program was working correctly, state points were calculated using  $NVT$  Monte Carlo,  $NPT$  Monte Carlo, and  $NVT$  Molecular Dynamics. Identical thermodynamic properties were obtained with all these techniques.

Because our primary intent was to compute the elastic constants, most simulations were performed on a relatively small system of 224 particles in a box with a size ratio of  $14:8\sqrt{3}$ . Two well-widths were chosen:  $\delta = 0.03$  and  $0.06$ , in units of  $\sigma$ .

**3.1. Calculation of the Bulk Modulus  $B$ .** The bulk modulus  $B = \mu + \lambda$  is given by

$$B = \rho \left( \frac{\partial P}{\partial \rho} \right) \quad (14)$$

where the pressure  $P$  is related to the trace of the stress tensor  $\mathcal{L}$  through  $P = -1/2 \mathcal{L}_{kk}$ . The reduced density is defined by  $\rho = N\sigma^2/A$ , where  $A$  is the system area and  $N$  the number of particles in the system. To determine the bulk modulus, the pressure tensor  $\mathcal{L}$  was measured as a function of the reduced density  $\rho$  and temperature  $T$  on a grid surrounding the solid–

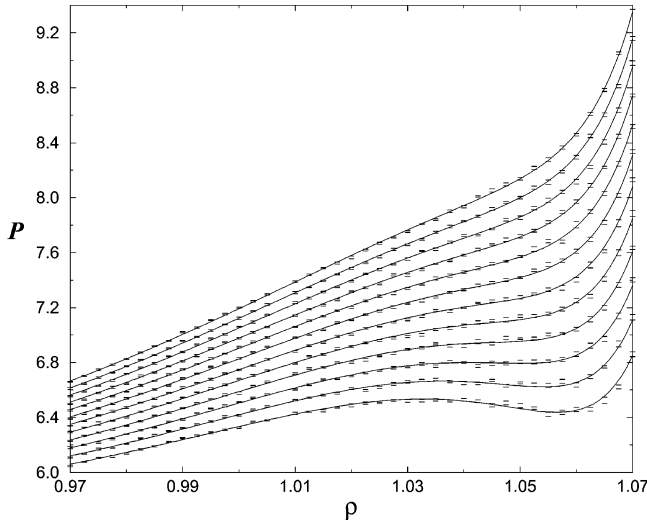


**Figure 2.** Measured equations of state for the square-well solid, and the fitted results, for  $\delta = 0.06$ . The different lines from the top of the figure correspond to the reduced temperatures 0.98–0.87 in steps of 0.01. The critical point is visible at  $T \approx 0.895$ ,  $\rho \approx 1.046$ . Pressure is measured in units of  $\epsilon\sigma^{-2}$ , density in units of  $\sigma^{-2}$ .

**TABLE 1: Fitting Parameters for the Pressure of a 2D Square-Well Fluid with  $\delta = 0.06^a$**

q	Fitting Parameter for Pressure				
	p = 0	p = 1	p = 2	p = 3	p = 4
0	69.24	-25.90	3.00	-0.127	-0.0001
1	-116.34	44.00	-4.23	-0.079	0.006
2	54.52	-19.70	1.74	-0.0017	-0.004

<sup>a</sup> See text.

**TABLE 2: Fitting Parameters for the Pressure of a 2D Square-Well Fluid with  $\delta = 0.03^a$**

q	Fitting Parameter for Pressure				
	p = 0	p = 1	p = 2	p = 3	p = 4
0	56013	11638	-895.42	30.2159	-0.3774
1	127520	-26497	2039.02	-68.82	0.8599
2	-72495	15065	-1159	39.13	-0.489

<sup>a</sup> See text.

solid critical point. Densities were varied in increments of 0.0025, and temperatures were varied in units of 0.01.

The pressure, as a function of temperature, was first reduced by the close-packed density  $\rho^* = \rho/\rho_{cp}$  and then fitted to a polynomial in  $\rho^*/(1 - \rho^*)$  and a simple power series in the temperature, i.e.,

$$P(\rho^*, T) = \sum_{p=0}^4 \sum_{q=0}^2 a_{pq} T^q \left( \frac{\rho^*}{1 - \rho^*} \right)^p \quad (15)$$

An example of the equations of state and the fit for  $\delta = 0.06$  is shown in Figure 2. Tables 1 and 2 show the fit parameters for the pressure for the two different square-well widths ( $\delta = 0.06$  in Table 1 and  $\delta = 0.03$  in Table 2). Having obtained the pressure, it is a simple matter to obtain the bulk modulus  $B$  by differentiation.

**3.2. Calculation of the Shear Modulus  $\mu$ .** The shear elastic constant ( $\mu$ ) was measured by imposing a small shear deformation  $\epsilon_{xy}$  on the system and measuring the response in the off-diagonal elements of the pressure tensor. The pressure tensor

**TABLE 3: Fitting Parameters for the Shear Modulus of a 2D Square-Well Fluid with  $\delta = 0.06^a$**

q	Fitting Parameter for Shear Modulus				
	p = 0	p = 1	p = 2	p = 3	p = 4
0	-1911.30	803.73	-119.58	7.272	-0.14
1	2203.56	-954.76	149.98	-9.871	0.231

<sup>a</sup> See text.

**TABLE 4: Fitting Parameters for the Shear Modulus of a 2D Square-Well Fluid with  $\delta = 0.03^a$**

q	Fitting Parameter for Shear Modulus				
	p = 0	p = 1	p = 2	p = 3	p = 4
0	-50882	10555	-775.191	23.8183	-0.2567
1	52482	-10833	791	-24.081	0.2589

<sup>a</sup> See text.

measured at a finite value of the strain can be related to first-order isothermal elastic constants  $C_{ij}^{(1)}$  at zero strain by<sup>47</sup>

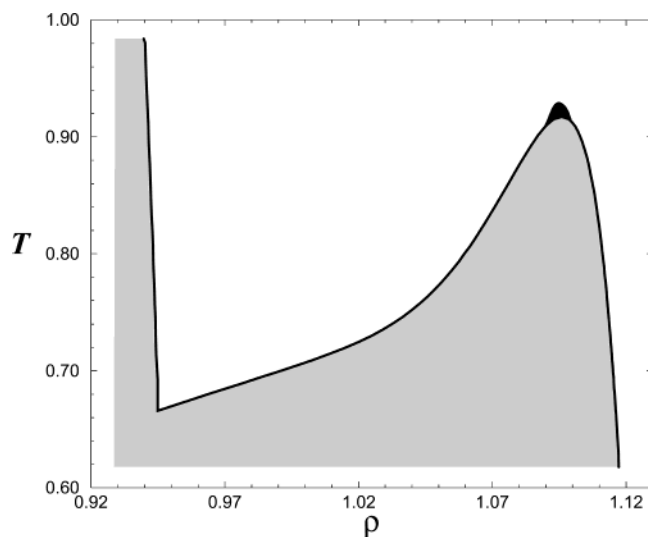
$$C^{(1)} = - \left( \frac{A'}{A} \right) (1 + \epsilon)^{-1} \mathcal{A} (1 + \tilde{\epsilon})^{-1} \quad (16)$$

where  $\epsilon$  is the matrix of deformations and  $\tilde{\epsilon}$  denotes its transpose.  $A$  and  $A'$  respectively denote the area and transformed area of the system, which are identical under shear deformation. The Lamé coefficient,  $\mu = C_{xyxy}$ , is then obtained by a linear fit of  $C_{xy}^{(1)}$  vs  $\epsilon_{xy}$ , the applied shear strain. The size of the applied shear must be chosen carefully. It must be sufficiently large that it produces a measurable response in the pressure tensor, but sufficiently small that the response produced is linear. Also, it must be small enough that no shear flow occurs during the simulation. The shear strain applied in any simulation was never more than 0.5%, and no evidence of shear flow was observed in the simulations. In practice, it is more important to obtain an accurate estimate of the bulk modulus in the critical region, because  $\mu$  remains high far from the melting line and increases monotonically as the density increases. The shear elastic constant was calculated for a similar (though coarser) grid of points in the  $(\rho, T)$  plane. Densities were varied in increments of 0.005, and temperatures were varied in units of 0.01. The shear modulus was fitted in the same way as the pressure. The fitted coefficients are tabulated in Tables 3 ( $\delta = 0.06$ ) and 4 ( $\delta = 0.03$ ).

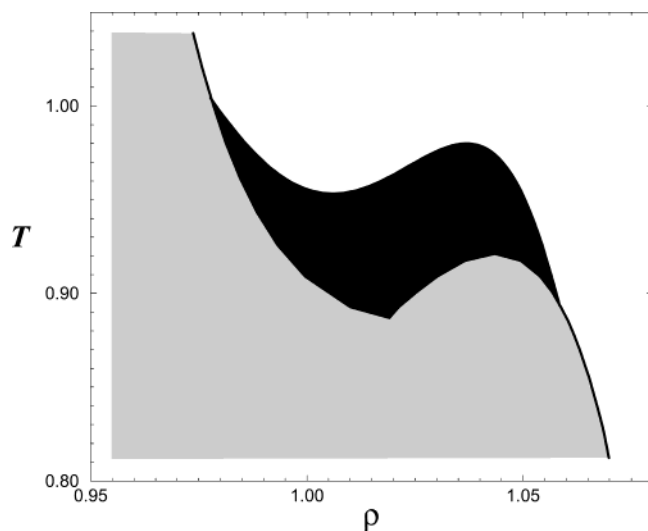
**3.3. Results.** Having obtained the bulk and shear moduli as a function of temperature and density near the critical point, it is a simple matter to evaluate  $K$  and delineate the region where  $K < 16\pi$ .

Figure 3 shows the phase diagram for  $\delta = 0.03$ . The phase diagram for this well width has been reproduced from the data presented in ref 41. Our data has been scaled so that the critical points occur at the same density and temperature. The critical temperature and density for the two well widths studied were  $T_c = 0.885$  and  $\rho_c = 1.01$ , respectively, for  $\delta = 0.03$  and  $T_c = 0.895$  and  $\rho_c = 1.046$ , respectively, for  $\delta = 0.06$ .

The region where the solid is unstable to dislocation unbinding has been shaded black, and the dislocation unbinding is localized to the region immediately surrounding the critical point. Figure 4 shows the phase diagram for  $\delta = 0.06$ . Here, the critical point is much closer to the melting line, and the triple-point temperature is much closer to the critical temperature  $T_c$ . The lower critical density for  $\delta = 0.06$  causes the bulk modulus  $B$  to be a much more slowly increasing function of density than is the case for  $\delta = 0.03$ . The system is “softer” and the region of unstable solid extends over a much larger



**Figure 3.** Phase diagram for the two-dimensional (2D) square-well system with  $\delta = 0.03$ . The region of unstable solid around the solid–solid critical point (the hexatic region) is shaded black. Regions of two-phase coexistence are shaded gray. The density and temperature are expressed in units  $\sigma^{-2}$  and  $\epsilon/k_B$ , respectively. At this high density, the critical point is far from the melting line confining the hexatic region to a small area around the critical point.



**Figure 4.** Phase diagram for the 2D square-well system with  $\delta = 0.06$ . The region of unstable solid around the solid–solid critical point (the hexatic region) is shaded black. Regions of two-phase coexistence are shaded gray. Units are as given in Figure 3. At this value of  $\delta$ , the critical temperature is near the triple-point temperature, causing the hexatic region to extend as far as the melting line.

region around the critical point. The effect of the approaching melting line is clearly visible. To the left of the critical point, the bulk modulus  $B$  is approximately constant, when compared to the rapid decrease of the shear modulus  $\mu$  with decreasing density. This reduces the value of  $K$  toward unstable values as the melting curve is approached. There is no evidence that the hexatic in this region melts via a disclination-unbinding mechanism. Rather, our simulations suggest that the hexatic phase undergoes a strong first-order transition to the isotropic fluid. However, it should be stressed that we have not studied the system-size dependence of the transition, nor have we performed a finite-size scaling analysis.

For such small systems, at high density, the defect density in our simulations was always zero. This greatly facilitated the numerical calculations, because the simulations could be

relatively short, since there was no need to equilibrate defect structures. Even for a system of 16 184 particles with  $\delta = 0.06$ , simulations showed that, at the critical point, the density of unbound dislocations is negligible. The low concentration of defects is, in fact, the prime feature that makes the present model a suitable candidate for exhibiting a true dislocation-unbinding transition, because it indicates that the dislocation core energy must be very large. In fact, by decreasing  $\delta$  and moving the solid–solid transition to higher densities, the core energy  $E_c$  can be made arbitrarily large.

Because there are, in practice, no defects in the system studied by simulation, the elastic constants that we measure are the “bare” or “unrenormalized” elastic constants of the Kosterlitz–Thouless theory. However, these represent an upper bound to the true, renormalized elastic constants of the infinite system. First, increasing the system size will reduce the elastic constants measured for the 224-particle system; longer-wavelength phonons will “soften” the system. This effect can easily be observed by measuring the pressure along an isotherm of a system of twice the linear extent of the 224-particle system. Second, and more importantly, the presence of defects *always* renormalizes  $K$  downward. This is particularly obvious in that portion of the phase diagram where we find  $K$  to be less than  $16\pi$ . In an infinite system, such values of  $K$  are renormalized to zero. Hence, the range of stability of the hexatic phase will be larger than that which follows from the present simulations. To see the physical manifestation of the hexatic phase, i.e., a power-law decay of orientational correlations, we need to simulate a system that is large enough to have unbound dislocation pairs. A calculation of the defect core energy will help us gain a better understanding of the system sizes needed to see a hexatic phase.

#### 4. Calculation of the Defect-Core Free Energy

The density of the hexatic phase near a solid–solid critical point can be high, compared to the density of the solid at the normal melting curve. This, coupled with the fact that the particle has a hard core, implies a very low dislocation density in the hexatic phase. In terms of the KTHNY theory, the dislocation fugacity is extremely small. We believe that the dislocation density may be so low in such a phase that we cannot observe it directly by simulation, at least using current computers. However, this by no means excludes experimental observation of such hexatic phases. A calculation of the dislocation core free energy will allow us to estimate the dislocation-pair density, as well as allowing quantitative comparison between different model potentials.

We stress that the Hamiltonian (eq 6) is a *free energy*, because it contains an explicit sum over all the degrees of freedom (the strain components) of the system. Several authors have reported calculations of the dislocation core energy. Fisher, Halperin, and Morf<sup>33</sup> calculated the dislocation core energy of a system of electrons ( $r^{-1}$  potential) and Joos and Duesbery for a system of Lennard-Jones particles.<sup>48</sup> Such calculations neglect the entropic contributions to the core energy and, therefore, focus on the zero-temperature properties of the dislocation. Hoover and Ladd calculated the core energy for a system with a piecewise linear force law, as well as the entropy using a quasi-harmonic approximation.<sup>32</sup> One only needs to consider a hard disk solid, in which *all* elastic properties arise from entropy alone to see that the entropic contributions cannot always be neglected, nor be approximated using a quasi-harmonic technique.

We follow the recipe of Fisher et al.<sup>33</sup> to calculate the core free energy. A system is created with two dislocations with

Burger's vectors of unit strength  $\mathbf{b}_1$  and  $\mathbf{b}_2$ , separated by a distance  $\mathbf{r}_{12}$ , with  $\mathbf{b}_1 = -\mathbf{b}_2$ . The free-energy difference between this system and a reference system with no dislocations is then measured. According to linear elasticity theory, this free-energy difference is

$$\mathcal{F}(\mathbf{b}_1, \mathbf{b}_2, \mathbf{r}_{12}, N, V, T) - \mathcal{F}(N, V, T) = \mathcal{F}^{\text{defect}} + \Delta\mathcal{F}^{\text{elastic}} + 2E_c \quad (17)$$

The quantity  $\mathcal{F}^{\text{defect}}$  is the contribution to the elastic free energy of the defects. It is not given simply by eq 8, because the defect interacts with all its periodic images, because of the periodic boundary conditions used in the simulation. The sum of the interactions of one defect with all its periodic images is only conditionally convergent, and Ewald summation must be used. The term  $\Delta\mathcal{F}^{\text{elastic}}$  is a measure of the difference between the elastic free energy of the system with and without a defect, and  $2E_c$  is the core free energy of the two dislocations, which is the quantity we wish to calculate. In this formulation, the core free energy has no dependence on the defect separation. This should hold if there is no interaction between defect cores. However, in a simulation, if the dislocations are too close, they will interact and the core free energy will be dependent on the dislocation separation. If the dislocations approach each other too closely, they can even annihilate each other. Therefore, to measure the core free energy, a series of measurements must be made with increasing dislocation separations. At sufficiently large separations, the core free energy will become independent of  $r$ ; this is *the* core free energy. A measure of the core size can be obtained from the distance at which this occurs.

Each stage of the calculation will be outlined below. Note that we must measure the free energy of a system constrained to have a constant pair of equal and opposite Burger's vectors, which is a nontrivial problem, because the dislocations attract each other and would become ultimately annihilated. Therefore, we need some mechanism of identifying and constraining dislocations in the lattice. First, we will address the right-hand side of eq 17, which represent the contributions to the free energy from continuum theory (see refs 32 and 33). Subsequently, we examine the techniques used to calculate the free energy of a system that contains two dislocations.

**4.1. Ewald Summation of Defect Energies.** The dislocation free energy (eq 8) is infinitely long-ranged. In a system with periodic boundary conditions, every dislocation interacts with all its periodic images. The total energy (per periodic block size  $L_x, L_y$ ) of an infinite array of dislocation pairs with Burger's vectors  $+\mathbf{b}$  and  $-\mathbf{b}$  at separation  $\mathbf{r}$  is given by

$$\mathcal{F}^{\text{defect}}(\mathbf{r}) = F_0^{\text{defect}}(\mathbf{r}) + \sum_{\mathbf{R} \neq 0} F_0^{\text{defect}}(\mathbf{R} - \mathbf{r}) - F_0^{\text{defect}}(\mathbf{R}) \quad (18)$$

where the sum is totalled over all  $\mathbf{R} = (l_x L_x, l_y L_y)$ , where  $l_x$  and  $l_y$  are integers and

$$F_0^{\text{defect}}(\mathbf{r}) = \frac{K}{8\pi} \sum_{\mathbf{r}_i \neq \mathbf{r}_j} \left[ \mathbf{b}_i \cdot \mathbf{b}_j \ln \left( \frac{r_{ij}}{a_0} \right) - \frac{(\mathbf{b}_i \cdot \mathbf{r}_{ij})(\mathbf{b}_j \cdot \mathbf{r}_{ij})}{r_{ij}^2} \right] \quad (19)$$

The sum can be made periodic by Ewald summation, in which the summation is split into two parts: a short-range part, which is summed in real space, and a long-range part that is summed in reciprocal space, both of which converge equally rapidly.

We refer the reader to refs 32 and 33 for more details. The result is

$$\mathcal{F}^{\text{defect}}(\mathbf{r}) = F_r(\mathbf{r}) + \sum_{\mathbf{R} \neq 0} [F_r(\mathbf{R} - \mathbf{r}) - F_r(\mathbf{R})] + \frac{1}{L_x L_y} \sum_{\mathbf{G} \neq 0} (e^{-i\mathbf{G}\mathbf{r}} - 1) F_k(\mathbf{G}) \quad (20)$$

where the real part of the sum is given by

$$F_r(\mathbf{r}) = \frac{K}{4\pi} \left\{ -\frac{b^2}{2} [E_1(\alpha r^2) + \ln \alpha + \gamma] - \left[ \frac{(\mathbf{b}\mathbf{r})^2}{r^2} \right] \exp(-\alpha r^2) \right\} \quad (21)$$

where  $E_1(x) = -Ei(-x)$  is the exponential integral and  $\gamma$  is Euler's constant. The  $k$ -space component of the sum is given by

$$F_k(\mathbf{k}) = \frac{K}{4\pi} \left[ \frac{\exp[-k^2/(4\alpha)]}{k^2} \right] 4\pi \left[ -b^2 + (\mathbf{b}\mathbf{k})^2 \left( \frac{1}{k^2} + \frac{1}{4\alpha} \right) \right] \quad (22)$$

With the choice of  $\alpha = \pi/(L_x L_y)$ , both sums converge equally rapidly. With the elastic constant  $K$  being known, it is a simple matter to calculate the sum in eq 20.

**4.2. Correction due to Unrelaxed Shear Strain.** Equation 17 implies that there is a decoupling between the contribution to the free energy from dislocations (eq 8) and the smoothly varying phonon modes (eq 7). Thus, there should be no difference in the linear elastic contribution of a system with and without dislocations. However, the pair of dislocations introduces an additional strain that cannot be relaxed in the simulation due to the periodic boundary conditions. This unrelaxed strain is

$$u_{ij} = \frac{1}{2} (\mathbf{b}_i \cdot \boldsymbol{\epsilon}_{jk} \mathbf{r}_k + \mathbf{b}_j \cdot \boldsymbol{\epsilon}_{ik} \mathbf{r}_k) \quad (23)$$

where  $\epsilon_{ij}$  is the Levi-Civita symbol. This results in an additional contribution to the free energy of

$$\Delta\mathcal{F}^{\text{elastic}} = \frac{1}{2} \mu b^2 \left( \frac{r^2}{L_x L_y} \right) \quad (24)$$

**4.3. Free-Energy Calculation with an Imposed Burger's Vector.** We wish to calculate the free energy of a system with two equal and opposite Burger's vectors at a fixed separation. Therefore, we need to be able to locate, characterize, and confine defects in our simulations and, subsequently, measure their free energy. We can locate and characterize defects using a combination of two techniques: Voronoi analysis and Burger's vector construction. We confine dislocations by fixing the magnitude of each dislocation's Burger's vector, and we measure the free energy of the system by a thermodynamic integration procedure.

**4.4. Burger's Vector Construction.** In continuum elastic theory, a Burger's vector is defined by integrating the displacement field around a closed curve in the medium:

$$\mathbf{b} = - \oint \frac{\partial \mathbf{u}}{\partial s} ds \quad (25)$$

If the integral is nonzero, the curve contains a dislocation of strength  $\mathbf{b}$ . We define the Burger's vector in a similar manner for a system made of particles. A circuit is taken, passing only

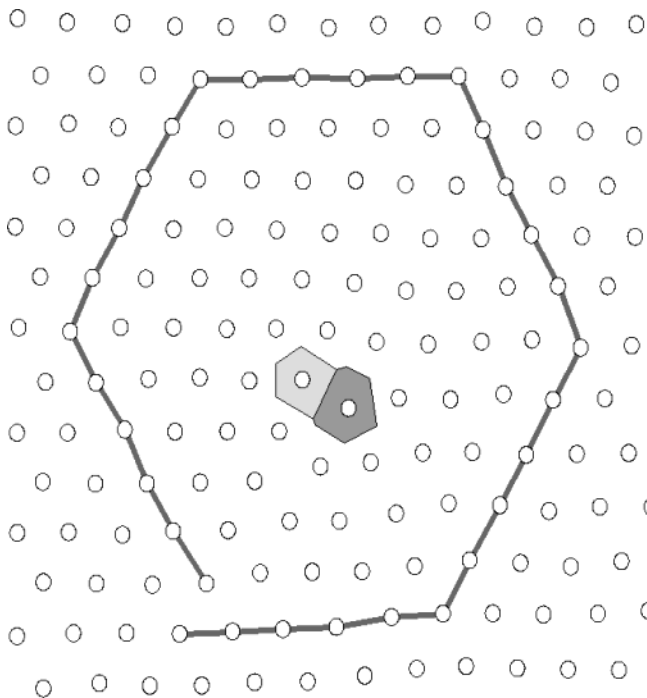


**Figure 5.** An isolated dislocation in a triangular lattice, identified by Voronoi and Burger's vector constructions. The Voronoi polyhedra are shown for all particles that have imperfect (i.e., different than 6-fold) coordination. The 5–7-coordinated pair characterizing the simplest isolated dislocation is clearly visible. A Burger's vector is shown with a path length of five steps. The path contains a single dislocation of strength one lattice unit, i.e.,  $\mathbf{b} = (-1/2, -\sqrt{3}/2)$  in Cartesian coordinates, if the Burger's vector path is taken counterclockwise.

through regions of perfect lattice. For our purposes, we use a Voronoi construction to define what constitutes a perfect lattice. If this circuit fails to close, the circuit contains a dislocation, the Burger's vector of which is the vector joining the starting and end points of the circuit (see Figure 5). In practice, because we will be required to define a Burger's vector dynamically during the course of a simulation, we need to be more specific about precisely how the circuit is taken. In the simulations described below, we used the following procedure to calculate a Burger's vector:

(1) The length of each side of the circuit is chosen, in units of  $a_0$ , the lattice spacing. A particle is chosen to be the starting point of the circuit and an initial walking direction,  $\hat{g}$ , is chosen along one of the lattice directions. We denote the current location on the circuit to be the *test particle*, which is located at  $r_i$ .

(2) The test particle is examined to determine if it is in a region of perfect lattice, i.e., if the particle has exactly six neighbors,  $j$ , identified by a Voronoi analysis. If it is not, the attempt at constructing a Burger's vector is abandoned.

(3) Denote the set of vectors that join the test particle to its six neighbors by  $r_{ij}$ . The possible locations for the next step of the walk are determined by forming the inner product of the current walking direction  $\hat{g}$  with  $\{r_{ij}\}$ . The particle that corresponds to the maximum value of  $\cos \phi = \hat{g} \cdot \hat{r}_{ij}$  is chosen to be the next step in the path (i.e., the new test particle), providing that  $\cos \phi > \sqrt{3}/2$ ; that is, the chosen direction is closer to the current walking direction than to any other lattice direction. If this criterion cannot be satisfied, the attempt at constructing a Burger's vector is abandoned.

(4) One step of the walk has been completed. We now must repeat the procedure for the next step of the walk, starting from the new test particle. If the end of one side of the hexagonal

circuit has been reached,  $\hat{g}$  is rotated in the positive sense by  $\pi/3$ . If the circuit is complete, the Burger's vector is calculated. Otherwise, the process is continued from step 4, which has been discussed previously.

Note that the definition of a dislocation by a Burger's vector is a collective property of a large group of atoms, namely all those contained within the circuit, whereas the Voronoi construction yields a microscopic, local definition of the defect structure that is based purely on coordination number. In the Voronoi picture, a dislocation can be identified with a pair of neighboring atoms with imperfect coordination. One of the pair has five neighbors, and the other has seven. Figure 5 shows this configuration with its associated Burger's vector. This should be considered to be the "ground state" of a dislocation; there are, of course, many different configurations of five, seven, and other coordination numbers that can describe a dislocation. Therefore, given a particular Voronoi tiling, it can be very difficult to identify where point defects are actually located, without using a Burger's vector construction to separate those groups that have no overall Burger's vector from those whose Burger's vectors are well-defined. For this reason, we prefer to use a Burger's vector description of a dislocation, because it imposes no particular coordination state on the system that we are simulating.

**4.5. Defect Creation.** Pairs of defects are created along the glide direction by applying a displacement field  $u(x,y)$  to a perfect lattice of coordinates scaled to lie between  $x, y \in (-0.5, 0.5)$ . The displacement field is of the form

$$u(x, y) = +k(1 - 2y)f(x) \quad (y > 0) \quad (26a)$$

$$= -k(1 + 2y)f(x) \quad (y < 0) \quad (26b)$$

where  $k$  is a suitably chosen constant and  $f(x)$  is some concave function symmetric about  $x = 0$  that vanishes at  $x = -0.5, 0.5$  (e.g.,  $\sin[(x + 0.5)\pi]$ ). The energy of the configuration generated in this fashion is then minimized by the steepest descents, using an  $r^{-n}$  potential to provide a starting configuration for subsequent simulations. Voronoi analysis showed that the resulting configuration contained two five–seven-coordinated dislocations separated along the glide direction by a distance of  $r \approx L_x/2$ , where  $L_x$  is the size of the simulation box in the  $x$ -direction. This corresponds to two Burger's vectors  $\mathbf{b} = (\pm 1, 0)$  at the given separation. Using this starting configuration in a standard Monte Carlo simulation, the defects annihilate each other after a few hundred simulation cycles. To generate configurations with different dislocation separations, configurations before annihilation were recorded and analyzed for the defect separation. To identify the location and separation of the dislocations, the Burger's vector was calculated as described previously, using every particle as the initial starting particle. Particle coordinates that produced (1,0) and (-1,0) were separately averaged to obtain the center of mass for each type of dislocation. The particle closest to the center of mass of each dislocation was chosen to be the starting point for determining the Burger's vector in the subsequent calculations to measure the free energy. Note that the center of mass of the dislocation as described does not correspond to the actual center of mass of the dislocation, because it includes a constant offset vector that translates the starting point to the center of the hexagonal path used to determine the Burger's vector.

**4.6. Monte Carlo Simulations at a Constant Burger's Vector.** To maintain a fixed value of the Burger's vector during a Monte Carlo simulation, we use the following technique. At regular intervals (once every Monte Carlo cycle, where one cycle

equals one move per particle), the entire configuration of the system is saved. Before saving the system, the Burger's vector is recalculated, using the stored initial starting points identified previously. If the Burger's vector has changed, the previous sequence of standard Metropolis Monte Carlo moves is rejected, and the system is restored to the previous saved configuration. The Burger's vector only changes slowly, and using this staged Monte Carlo technique, only needs to be recalculated infrequently. We find that the acceptance rate of cycles is  $\sim 50\%$ , depending on the density and type of system being investigated. The size of the path determining the Burger's vector determines the degree of constraint of the dislocation. If a very large path is used (of size six or more lattice units per side), the dislocations move toward each other (because of their mutual attraction) until they are confined the "wall" of the surrounding Burger's vector. To minimize this effect, the smallest possible Burger's vector was used, of three units per side, so that the dislocation was very tightly constrained and did not move during the simulation. During the course of the simulation, it was interesting to note the relaxation of the lattice surrounding the dislocations. Grain boundaries and bound dislocation pairs were formed, which screened the strong attraction of the dislocations.

**4.7. Free-Energy Calculation.** Using the Monte Carlo technique outlined previously, the free energy of a system that contains dislocations can be calculated using thermodynamic integration. By modifying the pair potential, a reversible path can be constructed between the solid that contains dislocations and a reference system of known free energy. We choose the reference system to be a harmonic, or Einstein, solid, where each particle is bound to its lattice site by a harmonic potential.<sup>49</sup> By increasing the strength of the coupling to the harmonic solid, the system can be made to freeze into a state in which the harmonic potential dominates. To reduce the square-well solid to a harmonic solid, it was first necessary to reduce the system to a hard-disk solid, because the presence of the nearby solid–solid critical point causes rapid variations in the square-well energy as the system is frozen. The modified interaction potential of the system is

$$U(\alpha, \gamma) = \sum_{i < j} [U^{\text{HD}} + \alpha U^{\text{SQ}}] + \gamma \sum_i (r_i - r_i^0)^2 \quad (27)$$

The hard-disk part of the potential  $U^{\text{HD}}$  is always left switched on;  $\alpha$  controls the effective square-well potential,  $U^{\text{SQ}}$ , and  $\gamma$  represents the coupling to the Einstein lattice position  $r_i^0$ . When  $\alpha = \gamma = 0$ , the system interacts via a hard-disk potential; with  $\alpha = 1, \gamma = 0$ , the system interacts via the full square-well potential; and when  $\alpha = 0, \gamma \neq 0$ , the hard-disk solid interacts with a harmonic solid with a coupling constant  $\gamma$ . To define the Einstein potential, it is necessary to have a reference lattice. For the systems that contain dislocations, the reference lattice was measured in a simulation with an unmodified square-well potential, with the mean positions defining  $r_i^0$ . Using the identity

$$\mathcal{F}(x_2) - \mathcal{F}(x_1) = \int_{x_1}^{x_2} dx \frac{\partial \mathcal{F}}{\partial x} \quad (28)$$

the free-energy difference between two states characterized by  $x$  can be measured. By setting  $\gamma$  to zero and varying  $\alpha$ , we obtain the difference between the square-well and hard-disk solids, namely

$$\Delta \mathcal{F}^{\text{HD}} = \mathcal{F}^{\text{SQ}} - \mathcal{F}^{\text{HD}} = \int_0^1 d\alpha \langle U^{\text{SQ}} \rangle_{(\alpha, \gamma=0)} \quad (29)$$

where  $\mathcal{F}^{\text{HD}}$  denotes the free energy of the square-well system ( $\alpha = 1, \gamma = 0$ ),  $\mathcal{F}^{\text{HD}}$  denotes that of the hard-disk system ( $\alpha = \gamma = 0$ ), and  $\langle \dots \rangle_{(\alpha, \gamma=0)}$  denotes an ensemble average sampled using the potential at the indicated values of  $\alpha$  and  $\gamma$ . Similarly, the free-energy difference between the hard-disk solid and a hard-disk solid strongly coupled to an Einstein lattice is

$$\begin{aligned} \Delta \mathcal{F}^{\text{HD+E}}(\gamma_{\text{max}}) &= \mathcal{F}^{\text{HD+E}}(\gamma_{\text{max}}) - \mathcal{F}^{\text{HD}} \\ &= \int_0^{\gamma_{\text{max}}} d\gamma \langle \sum_i (r_i - r_i^0)^2 \rangle_{(\alpha=0, \gamma)} \end{aligned} \quad (30)$$

If the coupling  $\gamma_{\text{max}}$  is very strong, the particles are bound extremely tightly to their lattice positions and rarely feel the hard-disk potential of their neighbors. The free-energy difference between this strongly coupled system and the reference system  $\mathcal{F}^{\text{E}}$  is simply

$$\Delta \mathcal{F}^{\text{UMB}} = \mathcal{F}^{\text{E}}(\gamma_{\text{max}}) - \mathcal{F}^{\text{HD+E}}(\gamma_{\text{max}}) \quad (31a)$$

$$= k_{\text{B}} T \ln \langle \exp[-\beta U(\alpha = 0, \gamma = \gamma_{\text{max}})] \rangle \quad (31b)$$

where the average is "umbrella-sampled", using the harmonic potential only. By evaluating these integrals using a series of simulations, the free-energy difference between the square-well system and the reference system can be calculated (and, hence, the absolute free energy of the square-well system).

There is one additional important point that has not yet been mentioned. The thermodynamic integration to the Einstein crystal must be performed in a system with a fixed center of mass. Without this constraint, the mean-square displacement would become on the order of  $L^2$  (where  $L$  is the box length) as  $\gamma \rightarrow 0$ , in which case the integrand of eq 30 would be sharply peaked around  $\gamma = 0$ , adversely affecting the accuracy of the integration. The details of performing a simulation at a fixed center of mass are given in ref 49. With this constraint, the free energy of the Einstein solid of  $N$  particles in a volume  $V$  becomes

$$\mathcal{F}^{\text{E}}(\gamma) = k_{\text{B}} T (N - 1) \ln \left( \frac{\pi}{\beta \gamma} \right) + k_{\text{B}} T \ln \left( \frac{N}{V} \right) \quad (32)$$

## 5. Free-Energy Calculation Results

The defect-core free energy was measured at one single state point for three different systems: the short-range attractive square-well system just above the solid–solid critical point, the equivalent hard-disk system, and, for comparison, a system interacting via a  $r^{-12}$  repulsive power potential (i.e., the pair potential is  $U(r) = \epsilon(\sigma/r)^{12}$ ). The state point chosen for the square-well system ( $\rho = 1.046, T = 0.9$ , and  $\delta = 0.06$ ) is inside the unstable regime, as determined by KTHNY theory. However, because of finite system size and the absence of (natural) dislocations, the elastic constants are still nonzero. The hard-disk core energies were obtained at the same density, as were those of the  $r^{-12}$  system, which was simulated at a reduced temperature ( $\beta\epsilon = 1$ ).<sup>36</sup> All systems simulated contained 1024 particles. The elastic constants for the square-well system were recomputed for the 1024 particle system at the state point that was simulated. The elastic constants for the hard-disk solid were computed using procedures that were identical to those described for the square-well solid (noted previously) and show good agreement with previous calculations.<sup>50</sup> For the  $r^{-12}$  system, the KTHNY constant  $K$  was taken from the paper of Broughton, Gilmer, and Weeks,<sup>38</sup> and the shear modulus  $\lambda$  obtained by linearly interpolating between two values measured at  $\rho = 1.06$

**TABLE 5: Contributions to the Core Free Energy of a Square-Well System with  $\delta = 0.06$  at  $T = 0.9$  and  $\rho = 1.046^a$** 

defect separation	$\Delta\mathcal{F}^{\text{HD}/N}$	$\Delta\mathcal{F}^{\text{HD+E}/N}$	$\mathcal{F}^{\text{E}/N}$	$\Delta\mathcal{F}^{\text{UMB}/N}$	$\mathcal{F}^{\text{Disl}}$	$\Delta\mathcal{F}^{\text{Shear}}$	$E_c^{\text{SQ}}$
0.00	-2.3005(4)	6.212(2)	10.890	$<10^{-4}$	0.00	0.00	$0.00 \pm 0$
4.48	-2.3260(3)	6.165(2)	10.890	$<10^{-4}$	0.86	1.12	$10.1 \pm 3$
6.44	-2.3297(3)	6.153(3)	10.890	$<10^{-4}$	1.45	2.31	$12.9 \pm 4$
8.51	-2.3313(3)	6.149(3)	10.890	$<10^{-4}$	1.86	4.03	$13.5 \pm 4$
11.37	-2.3381(2)	6.134(2)	10.890	$<10^{-4}$	2.18	7.20	$16.0 \pm 3$
14.52	-2.3399(4)	6.128(3)	10.890	$<10^{-4}$	2.33	11.42	$15.5 \pm 4$
15.49	-2.3393(9)	6.125(2)	10.890	$<10^{-4}$	2.35	13.35	$16.5 \pm 3$

<sup>a</sup> For a definition of the meanings of the symbols used in the table, see eqs 33 and 34.

**TABLE 6: Contributions to the Core Free Energy of a Hard-Disk System at  $\rho = 1.046^a$** 

defect separation	$\Delta\mathcal{F}^{\text{HD+E}/N}$	$\mathcal{F}^{\text{E}/N}$	$\Delta\mathcal{F}^{\text{UMB}/N}$	$\mathcal{F}^{\text{Disl}}$	$\Delta\mathcal{F}^{\text{Shear}}$	$E_c^{\text{HS}}$
0.00	6.212(2)	10.890	$<10^{-4}$	0.00	0.00	$0.00 \pm 0$
4.48	6.165(2)	10.890	$<10^{-4}$	15.6	1.91	$15.3 \pm 3$
6.44	6.153(3)	10.890	$<10^{-4}$	26.4	3.94	$14.5 \pm 4$
8.51	6.149(3)	10.890	$<10^{-4}$	33.7	6.90	$11.8 \pm 4$
11.37	6.134(2)	10.890	$<10^{-4}$	39.7	12.3	$13.9 \pm 3$
14.52	6.128(3)	10.890	$<10^{-4}$	42.5	20.1	$11.4 \pm 4$
15.49	6.125(2)	10.890	$<10^{-4}$	42.8	22.9	$11.4 \pm 3$

<sup>a</sup> For a definition of the meanings of the symbols used in the table, see eqs 33 and 34.

**TABLE 7: Contributions to the Core Free Energy of an  $r^{-12}$  System at  $T = 1.0$  and  $\rho = 1.046^a$** 

defect separation	$\Delta\mathcal{F}^{\text{R12+E}/N}$	$\mathcal{F}^{\text{E}/N}$	$\Delta\mathcal{F}^{\text{UMB}/N}$	$\mathcal{F}^{\text{Disl}}$	$\Delta\mathcal{F}^{\text{Shear}}$	$E_c^{\text{R12}}$
0.00	5.488(2)	8.847	1.670	0.00	0.000	$0.00 \pm 0$
4.48	5.492(2)	8.847	1.686	2.939	0.267	$5.2 \pm 3$
6.44	5.485(3)	8.847	1.683	4.967	0.550	$5.9 \pm 3$
8.51	5.488(2)	8.847	1.684	6.340	0.961	$4.4 \pm 3$
11.37	5.486(2)	8.847	1.688	7.454	1.717	$6.4 \pm 3$
14.52	5.508(2)	8.847	1.704	7.9903	2.801	$1.9 \pm 3$
15.49	5.498(3)	8.847	1.698	8.044	3.185	$4.0 \pm 4$

<sup>a</sup> For a definition of the meanings of the symbols used in the table, see eqs 33 and 34.

and  $\rho = 1.02$  was taken from the paper of Zollweg, Chester, and Leung.<sup>51</sup> Initial configurations that correspond to defect separations of  $\sim 4, 6, 8, 11, 14,$  and  $16$  lattice spacings were generated. For each initial configuration, the defect free energy was computed. Tables 5, 6, and 7 summarize the results for the square well, the hard disk, and the  $r^{-12}$  potential, respectively. The quantities  $\Delta\mathcal{F}^{\text{HD}}$  (which is the free-energy difference of the hard-disk and square-well system),  $\Delta\mathcal{F}^{\text{HD+E}}$  (which is the free-energy difference between the hard disk and strongly coupled harmonic solid),  $\mathcal{F}^{\text{E}}$  (which is the reference free energy), and  $\Delta\mathcal{F}^{\text{UMB}}$  (which represents the difference between the strongly coupled particles and the reference system) are all in units of free energy per particle. The quantities calculated using continuum theory— $\mathcal{F}^{\text{Dislocation}}$ , which is the Ewald summed dislocation free energy, and  $\Delta\mathcal{F}^{\text{Shear}}$ , which is the shear correction—are free energies per repeated periodic system. Hence, the absolute free energy is calculated, per particle, as

$$\mathcal{F}(\mathbf{b}_1, \mathbf{b}_2, \mathbf{r}_{12}, N, V, T) = \mathcal{F}^{\text{E}} + \Delta\mathcal{F}^{\text{HD}} - \Delta\mathcal{F}^{\text{HD+E}} - \Delta\mathcal{F}^{\text{UMB}} \quad (33)$$

and the core free energy is calculated as

$$E_c = \frac{1}{2}[N(\mathcal{F}(\mathbf{b}_1, \mathbf{b}_2, \mathbf{r}_{12}, N, V, T) - \mathcal{F}(N, V, T)) - \mathcal{F}^{\text{Dislocation}} - \mathcal{F}^{\text{Shear}}] \quad (34)$$

For the square-well system, the integral  $\Delta\mathcal{F}^{\text{HD}}$  was sampled

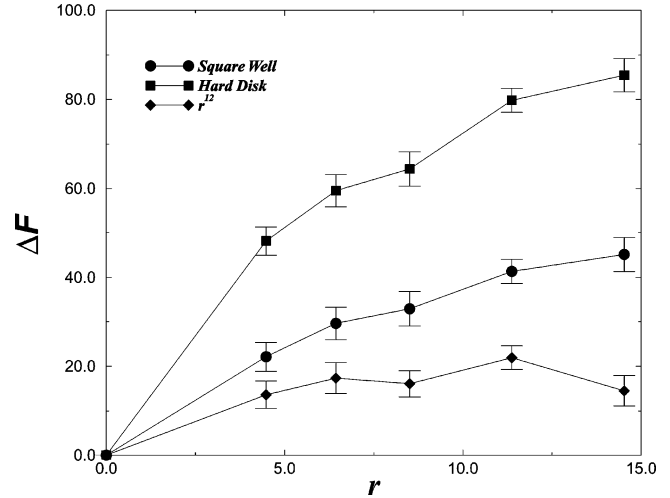


**Figure 6.** Free-energy difference of systems with and without dislocations at a separation  $r$ . The three systems are as follows: the square-well system with  $\delta = 0.06$  at  $T = 0.9$  and  $\rho = 1.046$ , near the critical point of the solid–solid transition; the equivalent hard-disk system at the same density; and an  $r^{-12}$  system at the same density with a temperature of  $T = 1$ . The defect core energies are given in units of  $k_B T / \epsilon$ , and the defect separation is given in units of the lattice spacing  $a_0$ .

by varying  $\alpha$  between (0,1) in steps of 0.1. The integral  $\Delta\mathcal{F}^{\text{HD+E}}$  was sampled, for the square-well and hard-disk system, with the set of points  $\gamma = 0, \gamma = \sum_{i=1,12} e^i$ , and the equivalently named  $\Delta\mathcal{F}^{\text{R12+E}}$  for the  $r^{-12}$  system was sampled with the set  $\gamma = 0, \gamma = \sum_{i=1,10} e^i$ .

The difference in the free energy of the dislocation and reference systems is shown in Figure 6. The core free energy is shown in Figure 7. The errors shown in the core energy are entirely due to the uncertainty in the determination of the free energy of the defect and reference systems. The defect-core energy is determined from the difference of two similarly sized quantities; the free energies of the defect and reference systems, where the difference is only slightly larger than the noise. The error in the free energy per particle remains approximately constant with increasing system size; however, the defect-core free energy is spread over more particles. Therefore, estimating the defect-core free energy by this technique is limited to a narrow range of system sizes: those large enough to support a defect, and those small enough that the dislocation free energy is not lost in the noise. We found that doubling the number of particles to 2304 ( $48 \times 24$  unit cells), significantly worsened the results, whereas the range of dislocation separation available in a system of 576 particles ( $24 \times 12$  unit cells) was insufficient to observe clear trends in the defect free energies as a function of  $r$ . Nevertheless, the defect core energies show clear systematic trends. Near a dislocation, there are large strain gradients; locally, the system is very deformed. The core energy is

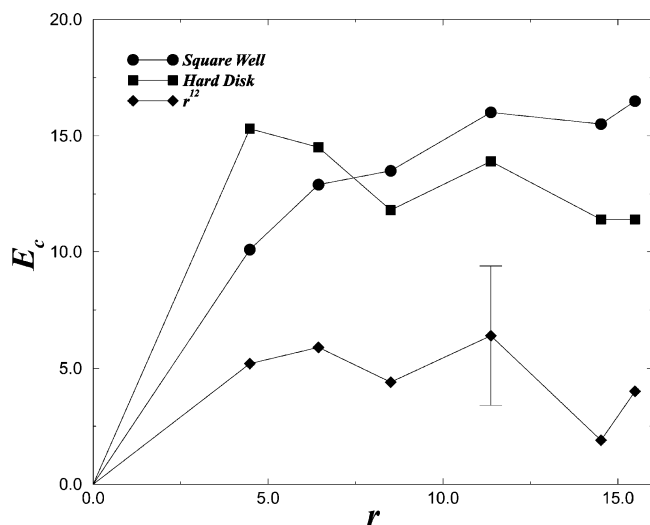


**Figure 7.** Plots of the defect core energies versus the dislocation separation for three different systems: the square-well system with  $\delta = 0.06$  at  $T = 0.9$  and  $\rho = 1.046$  near the critical point of the solid–solid transition, the equivalent hard-disk system at the same density, and an  $r^{-12}$  system at the same density with a temperature of  $T = 1$ . The defect core energies are given in units of  $k_B T/\epsilon$ , and the defect separation is given in units of the lattice spacing  $a_0$ . The results are presented for a simulation of a system of 1024 particles.

determined by how the system relaxes these strain gradients. In a hard-core system, strain can only be relaxed within the confines of surrounding hard cores. The strain is transmitted a large distance, and the free energy increases because of the extra confinement of many particles. For the  $r^{-12}$  system, the system can relax strains by locally increasing the potential energy, which leads to a smaller defect core with a lower free energy. For the square-well system, the core energy is dominated by the free-energy difference of the dislocation and reference systems. Because  $K$  is so small, the smoothly varying contribution from the dislocations is rather insignificant. The contribution from the unrelaxed shear indicates that, although  $K$  is small, the shear modulus  $\lambda$  is still relatively large. For the hard-disk system,  $K$  is very large and much of the free-energy difference is accounted for by the linear elastic dislocation and shear free energy. In this sense, the hard-disk system is described better by linear elastic theory in this distance regime than the square-well system. The  $r^{-12}$  system, on the other hand, seems to show no systematic increase of the free-energy difference or core energy past  $r = 5$  lattice units. The core size is smaller, as is the core free energy, compared to the systems that possess a hard core. Therefore, it is much easier to create defects in this system.

We see that, for the square-well system, at a point where the elastic constant  $K$  indicates the solid will become unstable to dislocation unbinding, the defect-core free energy is extremely high. Therefore, it is valid to apply the Halperin and Nelson theory, which relies upon an expansion in the parameter  $y = \exp[-E_c/(k_B T)]$  in this region of the phase diagram. This is the reason that we feel justified in calling our unstable region a “hexatic” phase. Other systems that fulfill the criteria for instability (i.e.,  $K < 16\pi$ ) may not have a sufficiently high core energy for the theory of Halperin and Nelson to be strictly valid in this regime. The value of the core energy gives an indication of the defect density in the system; it is very difficult for the system to have a fluctuation of the size  $\sim 15k_B T$ . Fisher et al. calculated the defect density by assuming that pairs of defects form diatomic molecules that do not interact with each other.

The density of dislocation pairs per simulation box ( $\rho^{\text{box}}$ ) then is<sup>33</sup>

$$\rho^{\text{box}} = \exp\left(-\frac{2E_c}{k_B T}\right) Z(K) \quad (35)$$

where  $Z(K)$  is the internal partition function of a dislocation pair:

$$\begin{aligned} Z(K) &= 3 \int_{r < r_{\min}} \frac{dr}{A} \exp\left\{-\frac{K}{4\pi} \left[ \ln\left(\frac{r}{a_0}\right) - \frac{(b \cdot r)^2}{r^2} \right]\right\} \\ &= \frac{4\pi\sqrt{3}}{K/4\pi - 2} \left(\frac{r_{\min}}{a_0}\right)^{2-K/(4\pi)} I_0\left(\frac{K}{8\pi}\right) \exp\left(\frac{K}{8\pi}\right) \end{aligned} \quad (36)$$

The quantity  $r_{\min}$  is a measure of the “core size” of a dislocation, and  $I_0$  is a modified Bessel function.  $Z(K)$  is of  $O(1)$  if  $K \approx 16\pi$ ; therefore,  $\rho^{\text{box}} \approx \exp[-2E_c/(k_B T)]$ . Therefore, the defect-pair density for the square-well system is  $e^{-30}$  (i.e., extremely small). This presupposes that the effect of finite system size on the core free-energy calculation is negligible. As discussed previously, a finite size scaling analysis of the dislocation core free energy would be impractical, because of the technical difficulties of measuring the core free energy in larger systems. Examination of Figure 7 shows that, for the square-well system, the independence of the core energy of the dislocation separation is not clear. The measured core free energy is an upper bound on the true, system-size-independent, core free energy; the effect of a small system is to force a rapid decay of strains around a dislocation, so that the strained lattice can be accommodated in the periodic cell. Increasing the system size reduces these strain gradients toward values that are adequately described by eq 18 and, hence, reduces the amount of free energy that must be accounted for by the dislocation core. In any case, the density of dislocations predicted by our simulations is extremely low. Even in an experiment, the possibility of observing spontaneous dislocation nucleation in an equivalent square-well colloid system (for instance, a colloid–polymer mixture) would be remote. However, we should expect the core energy of dislocations to decrease rapidly with density. Hence, for a system with a wider attractive well, which has a solid–solid transition close to the melting line, free dislocations are much more likely to be found in experiments.

## 6. Conclusions

We have shown that the presence of an isostructural critical point in the two-dimensional solid phase can result in dislocation-unbinding instability, in a region that is guaranteed to be otherwise thermodynamically stable. Because of the very high core free energy in this region, which is principally due to the presence of the harsh repulsion between particles, the system will become hexatic at sufficiently large system sizes. Calculation of the defect free energy of three systems—the square-well solid near the solid–solid critical point, the hard-disk solid at the same density, and an  $r^{-12}$  solid—shows that the presence of a harsh repulsion significantly increases the core free energy, resulting in a much lower defect concentration for a given density.

**Acknowledgment.** We thank Angelo Cacciuto for a critical reading of this manuscript. This work is part of the research program of the Foundation for Fundamental Research of Matter (FOM) and is supported financially by The Netherlands Organization for Scientific Research (NWO). P.B. acknowledges

NATO/EPSC for support and the FOM Institute for its hospitality during his stay.

## References and Notes

- (1) Peierls, R. *Surprises in Theoretical Physics*; Princeton University Press: Princeton, NJ, 1979.
- (2) Kosterlitz, J. M.; Thouless, D. J. *J. Phys. C* **1972**, *5*, L124; **1973**, *6*, 1181.
- (3) Halperin, B. I.; Nelson, D. R. *Phys. Rev. Lett.* **1978**, *41*, 121. Nelson, D. R.; Halperin, B. I. *Phys. Rev. B* **1979**, *19*, 2457.
- (4) For a recent review, see: Glaser, M. A.; Clark, N. A. *Adv. Chem. Phys.* **1993**, *83*, 543 and references therein.
- (5) Strandburg, K. J., Ed. *Bond-Orientational Order in Condensed Matter Systems*; Springer: New York, 1992.
- (6) Weber, H.; Marx, D. *Europhys. Lett.* **1994**, *27*, 593.
- (7) Kusner, R. E.; Mann, J. A.; Kerins, J.; Dahm, A. J. *Phys. Rev. Lett.* **1994**, *73*, 3113.
- (8) Chen, K.; Kaplan, T.; Mostoller, M. *Phys. Rev. Lett.* **1995**, *74*, 4019.
- (9) Morales, J. J.; Velasco, E.; Toxvaerd, S. *Phys. Rev. E* **1994**, *50*, 2844.
- (10) Fernández, J. F.; Alonso, J.; Stankiewicz, J. *Phys. Rev. Lett.* **1995**, *75*, 3477.
- (11) Bagchi, K.; Andersen, H. C.; Swope, W. *Phys. Rev. Lett.* **1996**, *76*, 255.
- (12) Murray, C. A. Faceting in Bond-Oriented Glasses and Quasicrystals (Chapter 4). In *Bond-Orientational Order in Condensed Matter Systems*; Strandburg, K. J., Ed.; Springer: New York, 1992; pp 137–215.
- (13) Marcus, A. H.; Rice, S. A. *Phys. Rev. Lett.* **1996**, *77*, 2577–2580.
- (14) Marcus, A. H.; Rice, S. A. *Phys. Rev. E* **1997**, *55*, 637–656.
- (15) Zangi, R.; Rice, S. A. *Phys. Rev. E* **1998**, *58*, 7529–7544.
- (16) Zahn, K.; Maret, G. *Phys. Rev. Lett.* **2000**, *85*, 3656–3659.
- (17) Zahn, K.; Wille, A.; Maret, G.; Sengupta, S.; Nielaba, P. *Phys. Rev. Lett.* **2003**, *90*, 155506.
- (18) Grier, D. G.; Murray, C. A.; Bolle, C. A. *Phys. Rev. Lett.* **1991**, *66*, 2270–2273.
- (19) Murray, C. A.; Gammel, P. L.; Bishop, D. J. *Phys. Rev. Lett.* **1990**, *64*, 2312–2315.
- (20) Huang, C. C. Experimental Studies of Melting and Hexatic Order in Two-Dimensional Colloidal Suspensions (Chapter 3). In *Bond-Orientational Order in Condensed Matter Systems*; Strandburg, K. J., Ed.; Springer: New York, 1992; pp 78–136.
- (21) Somer, F. L., Jr.; Canright, G. S.; Kaplan, T.; Chen, K.; Mostoller, M. *Phys. Rev. Lett.* **1997**, *79*, 3431–3434.
- (22) Jaster, A. *Phys. Rev. E* **1999**, *59*, 2594–2602.
- (23) Sengupta, S.; Nielaba, P.; Binder, K. *Phys. Rev. E* **2000**, *61*, 6294–6301.
- (24) Binder, K.; Sengupta, S.; Nielaba, P. *J. Phys. Condens. Matter* **2002**, *14*, 2323–2333.
- (25) Bates, M. A.; Frenkel, D. *Phys. Rev. E* **2000**, *61*, 5223–5227.
- (26) Chekmarev, D. S.; Oxtoby, D. W.; Rice, S. A. *Phys. Rev. E* **2001**, *63*, 051502.
- (27) Jaster, A. J. *Europhys. Lett.* **1998**, *42*, 277–281.
- (28) Chui, S. T. *Phys. Rev. B* **1982**, *28*, 178.
- (29) Saito, Y. *Phys. Rev. B* **1982**, *26*, 6239.
- (30) Bladon, P.; Frenkel, D. *Phys. Rev. Lett.* **1995**, *74*, 2519.
- (31) Chou, T.; Nelson, D. R. *Phys. Rev. E* **1996**, *53*, 2560–2570.
- (32) Ladd, A. J. C.; Hoover, W. G. *Phys. Rev. B* **1982**, *26*, 5469.
- (33) Fisher, D. S.; Halperin, B. I.; Morf, R. *Phys. Rev. B* **1979**, *20*, 4692.
- (34) Landau, L. D.; Lifshitz, E. M. *Theory of Elasticity*; Pergamon Press: New York, 1970.
- (35) Nabarro, F. R. N. *Theory of Dislocations*; Clarendon: Oxford, U.K., 1967.
- (36) Young, A. P. *Phys. Rev. B* **1979**, *19*, 1855.
- (37) Swope, W. C.; Andersen, H. C. *J. Chem. Phys.* **1995**, *102*, 2851.
- (38) Broughton, J. Q.; Gilmer, G. H.; Weeks, J. D. *Phys. Rev. B* **1982**, *25*, 4651.
- (39) Allen, M. P.; Frenkel, D.; Gignac, W. *J. Chem. Phys.* **1983**, *78*, 4206.
- (40) Hagen, M. H. J.; Frenkel, D. *J. Chem. Phys.* **1994**, *101*, 4093. Mederos, L.; Navascues, G. *J. Chem. Phys.* **1994**, *101*, 9841. Ilett, S. M.; Orrock, A.; McPoon, W. C. K.; Pusey, P. N. *Phys. Rev. E* **1995**, *51*, 1344. Coussaert, T.; Baus, M. *Phys. Rev. E* **1995**, *52*, 862. Gilvillegas, A.; Vega, C.; Delrio, F.; Malijevsky, A. *Mol. Phys.* **1995**, *86*, 857.
- (41) Bolhuis, P.; Frenkel, D. *Phys. Rev. Lett.* **1994**, *72*, 2211. Bolhuis, P.; Hagen, M.; Frenkel, D. *Phys. Rev. E* **1994**, *50*, 4880.
- (42) Daanoun, A.; Tejero, C. F.; Baus, M. *Phys. Rev. Lett.* **1994**, *73*, 752. Daanoun, A.; Tejero, C. F.; Lekkerkerker, H. N. W.; Baus, M. *Phys. Rev. E* **1994**, *50*, 2913.
- (43) Likos, C. N.; Németh, Zs. T.; Löwen, H. *J. Phys. Condens. Matter* **1994**, *6*, 10965.
- (44) Prost, J.; Toner, J. *Phys. Rev. A* **1987**, *36*, 5008.
- (45) Alder, B. J.; Wainwright, T. E. *J. Chem. Phys.* **1959**, *31*, 459.
- (46) Rapaport, D. C. *J. Comput. Phys.* **1980**, *34*, 184.
- (47) See, for example: Frenkel, D. In *Simple Molecular Systems at Very High Density*; Polian, A., Loubeyre, P., Boccara, N., Eds.; Plenum: New York, 1988.
- (48) Joos, B.; Duesbery, M. S. *Phys. Rev. Lett.* **1985**, *55*, 1997.
- (49) Frenkel, D.; Ladd, A. J. C. *J. Chem. Phys.* **1984**, *81*, 3188.
- (50) Wojciechowski, K. W.; Branka, A. C. *Phys. Lett. A* **1988**, *134*, 314.
- (51) Zollweg, J. A.; Chester, G. V.; Leung, P. W. *Phys. Rev. B* **1989**, *39*, 9518.
- (52) Zollweg, J. A.; Chester, G. V. *Phys. Rev. B* **1992**, *46*, 11186.